Macrophage migration inhibitory factor promotes cyst growth in polycystic kidney disease

Li Chen, Xia Zhou, Lucy X. Fan, Ying Yao, Katherine I. Swenson-Fields, Mihaela Gadjeva, Darren P. Wallace, Dorien J.M. Peters, Alan Yu, Jared J. Grantham, Xiaogang Li

Research Article **Nephrology**

Autosomal dominant polycystic kidney disease (ADPKD) is characterized by renal cyst formation, inflammation, and fibrosis. Macrophages infiltrate cystic kidneys, but the role of these and other inflammatory factors in disease progression are poorly understood. Here, we identified macrophage migration inhibitory factor (MIF) as an important regulator of cyst growth in ADPKD. MIF was upregulated in cyst-lining epithelial cells in polycysitn-1–deficient murine kidneys and accumulated in cyst fluid of human ADPKD kidneys. MIF promoted cystic epithelial cell proliferation by activating ERK, mTOR, and Rb/E2F pathways and by increasing glucose uptake and ATP production, which inhibited AMP-activated protein kinase signaling. MIF also regulated cystic renal epithelial cell apoptosis through p53-dependent signaling. In polycystin-1–deficient mice, MIF was required for recruitment and retention of renal macrophages, which promoted cyst expansion, and *Mif* deletion or pharmacologic inhibition delayed cyst growth in multiple murine ADPKD models. MIF-dependent macrophage recruitment was associated with upregulation of monocyte chemotactic protein 1 (MCP-1) and inflammatory cytokine TNF-α. TNF-α induced MIF expression, and MIF subsequently exacerbated TNF-α expression in renal epithelial cells, suggesting a positive feedback loop between TNF-α and MIF during cyst development. Our study indicates MIF is a central and upstream regulator of ADPKD pathogenesis and provides a rationale for further exploration of MIF as a therapeutic target for ADPKD.

Find the latest version:

https://jci.me/80467/pdf

Macrophage migration inhibitory factor promotes cyst growth in polycystic kidney disease

Li Chen,[1,2,4] Xia Zhou,[1,2] Lucy X. Fan,[1,2] Ying Yao,[1,2] Katherine I. Swenson-Fields,[2,3] Mihaela Gadjeva,[5] Darren P. Wallace,[1,2] Dorien J.M. Peters,[6] Alan Yu,[1,2] Jared J. Grantham,[1,2] and Xiaogang Li[1,2,3]

[1]Department of Internal Medicine, [2]Kidney Institute, and [3]Department of Anatomy and Cell Biology, University of Kansas Medical Center (KUMC), Kansas City, Kansas, USA. [4]Department of Clinical Laboratory, Tongji Hospital, Huazhong University of Science and Technology, Wuhan, China. [5]Department of Medicine, Brigham and Women's Hospital, Harvard Medical School, Boston, Massachusetts, USA. [6]Department of Human Genetics, Leiden University Medical Center, Leiden, Netherlands.

Autosomal dominant polycystic kidney disease (ADPKD) is characterized by renal cyst formation, inflammation, and fibrosis. Macrophages infiltrate cystic kidneys, but the role of these and other inflammatory factors in disease progression are poorly understood. Here, we identified macrophage migration inhibitory factor (MIF) as an important regulator of cyst growth in ADPKD. MIF was upregulated in cyst-lining epithelial cells in polycysitn-1–deficient murine kidneys and accumulated in cyst fluid of human ADPKD kidneys. MIF promoted cystic epithelial cell proliferation by activating ERK, mTOR, and Rb/E2F pathways and by increasing glucose uptake and ATP production, which inhibited AMP-activated protein kinase signaling. MIF also regulated cystic renal epithelial cell apoptosis through p53-dependent signaling. In polycystin-1–deficient mice, MIF was required for recruitment and retention of renal macrophages, which promoted cyst expansion, and *Mif* deletion or pharmacologic inhibition delayed cyst growth in multiple murine ADPKD models. MIF-dependent macrophage recruitment was associated with upregulation of monocyte chemotactic protein 1 (MCP-1) and inflammatory cytokine TNF-α. TNF-α induced MIF expression, and MIF subsequently exacerbated TNF-α expression in renal epithelial cells, suggesting a positive feedback loop between TNF-α and MIF during cyst development. Our study indicates MIF is a central and upstream regulator of ADPKD pathogenesis and provides a rationale for further exploration of MIF as a therapeutic target for ADPKD.

Introduction

Autosomal dominant polycystic kidney disease (ADPKD) is an inherited disease characterized by formation and progressive growth of innumerous cysts and is associated with renal interstitial inflammation and fibrosis. ADPKD is caused by mutations in *PKD1* and *PKD2*, genes that encode polycystin-1 (PC1) and polycystin-2 (PC2), respectively (1). Multiple signaling pathways have been identified in regulating cystic renal epithelial cell proliferation and apoptosis, and targeting these pathways delays cyst growth in animal models of PKD (2–4). Interstitial inflammation, which has been consistently reported in human and animal models of PKD, also regulates cyst growth and is associated with functional impairment. The selective depletion of macrophages in kidneys of *Pkd1* conditional KO mice and congenital polycysitic kidney (*cpk*) mice caused a significantly lower cystic index, reduced proliferation of cyst-lining cells, and improved renal function (5, 6). However, the mechanisms promoting recruitment of macrophages to pericystic and interstitial sites within cystic kidneys, and the specific roles macrophages and other infiltrating inflammatory cells play in cystogenesis, have not been defined.

Macrophage migration inhibitory factor (MIF) as a pleiotropic proinflammatory cytokine (7), possessing tautomerase activity,

plays an important role in the recruitment of innate and adaptive immune cells to sites of inflammation (8). MIF was originally identified as a soluble factor in the culture medium of activated T lymphocytes that inhibited the random migration of macrophages. In addition to T lymphocytes, MIF is also expressed and secreted by other cell populations, including macrophages/monocytes (9, 10), endothelial cells (ECs) (11), epithelial cells (12), smooth muscle cells (13), synovial fibroblasts (14), and anterior pituitary cells (14). In adults, the predominant sites of MIF expression are the proliferating and differentiating epithelial linings of various organs (15). The broad expression of MIF suggests that it is involved in a wide array of physiological and pathophysiological processes.

MIF plays a critical pathogenic role in kidney diseases through mechanisms involving the innate and adaptive immune systems; the induction of cytokines, chemokines, and adhesion molecules; and interactions with glucocorticoids and the hypothalamic-pituitary–adrenal axis (16). High MIF production is found in human and experimental kidney disease and contributes to macrophage and T cell accumulation, as well as progressive renal injury (16). Upregulation of MIF was also reported in the kidney tissue of IgA nephropathy patients, compared with healthy controls and patients with anti-neutrophil cytoplasmic antibody–associated (ANCA-associated) glomerulonephritis (17). The functional importance of MIF in kidney disease is demonstrated by the findings that treatment with a neutralizing anti-MIF antibody prevents or reverses renal injury in crescentic anti-GBM glomerulonephritis (18). In addition, mice null for MIF are protected against immune-mediated lupus nephritis (19).
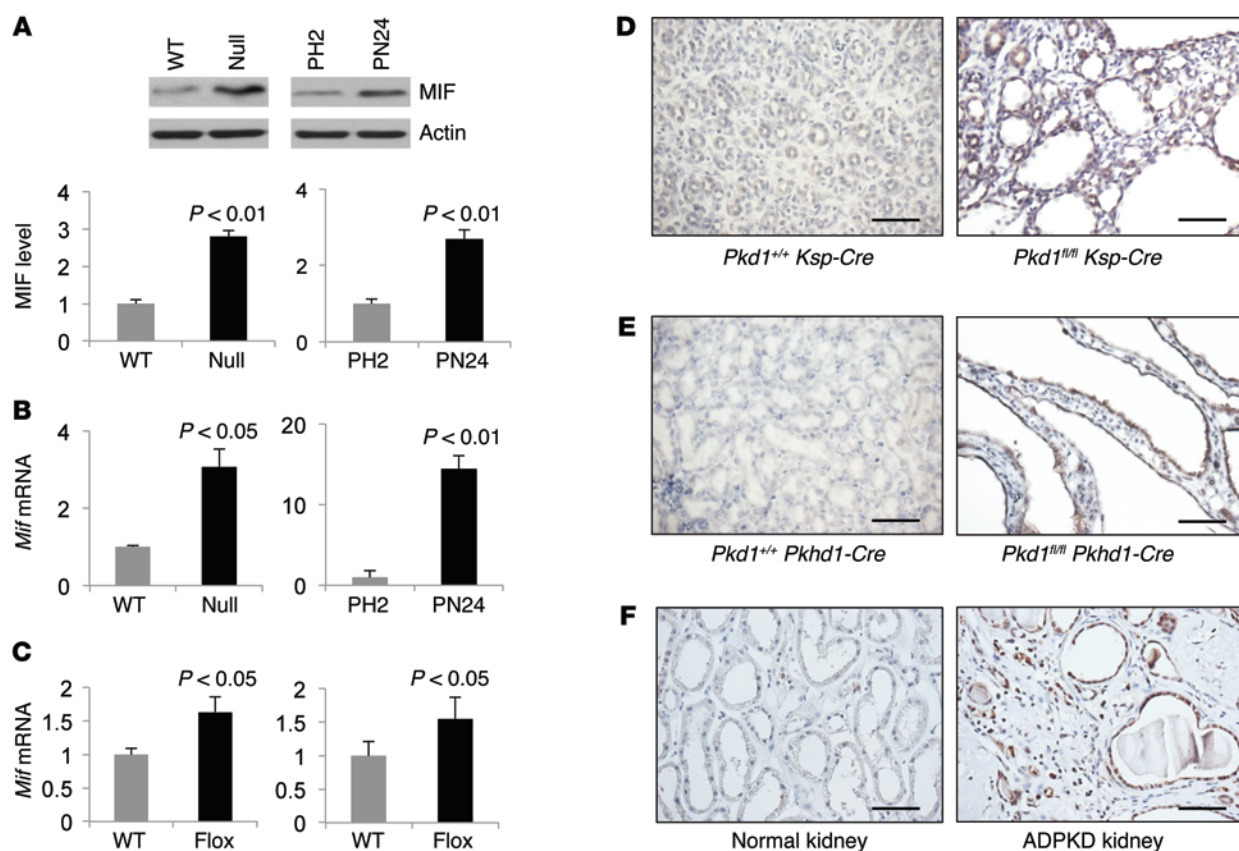
Figure 1. *Pkd1* mutant renal epithelial cells and tissues demonstrated increased expression of MIF. (**A**) Western blot analysis of the expression of MIF from whole-cell lysates of *Pkd1* (WT) and *Pkd1^{null/null}* (Null) MEK cells, as well as in postnatal *Pkd1* heterozygous PH2 (PH2) cells and *Pkd1* homozygous PN24 (PN24) cells. The expression of MIF was quantified from 3 independent immunoblots and was presented as the relative expression level of MIF standardized to actin in the bottom panel. $P < 0.01$. (**B**) qRT-PCR analysis of the expression of *Mif* mRNA in *Pkd1* (WT) and *Pkd1^{null/null}* (Null) MEK cells ($P < 0.05$), as well as in postnatal *Pkd1* heterozygous PH2 (PH2) cells and *Pkd1* homozygous PN24 (PN24) cells ($P < 0.01$). $n = 3$. (**C**) qRT-PCR analysis of the expression of *Mif* mRNA in PN7 kidneys from *Pkd1^{+/+} Ksp-Cre* (WT) and *Pkd1^{fl/fl} Ksp-Cre* (Flox) neonates (left panel) ($P < 0.05$) and in PN25 kidneys from *Pkd1^{+/+} Pkhd1-Cre* (WT) and *Pkd1^{fl/fl} Pkhd1-Cre* (Flox) mice (right panel) ($P < 0.05$). $n = 3$. Statistical analysis was performed using an unpaired 2-tailed Student's *t* test. (**D**–**F**) MIF expression was increased in *Pkd1* mutant kidney tissues as examined by immunohistochemical staining with anti-MIF antibody in PN7 kidney sections from *Pkd1^{+/+} Ksp-Cre* and *Pkd1^{fl/fl} Ksp-Cre* neonates (**D**), in PN25 kidney sections from *Pkd1^{+/+} Pkhd1-Cre* and *Pkd1^{fl/fl} Pkhd1-Cre* mice (**E**), as well as in kidney sections from normal and ADPKD kidneys (**F**). Scale bars: 100 μm.

MIF is considered an important therapeutic target for treating inflammatory diseases, autoimmune diseases, neoplasia, and cancer. MIF regulates the cellular activities through transcriptional regulation of inflammatory gene products; modulation of cell proliferation, differentiation, cell cycle control, and metabolism; and inhibition of apoptosis (8). The proteins and pathways regulated by MIF include SRC, ERK, mTOR, AMPK, Rb, AKT, and p53, as well as TNF-α and monocyte chemotactic protein 1 (MCP-1) in different cell types (20–28). Notably, all the proteins and pathways listed are hyperactive in PKD (2, 3, 29–35). However, the functional roles of MIF in regulating the interplay among these signaling pathways and in regulating the processes — including glucose uptake and macrophage recruitment in a single cell type, e.g., renal epithelial cells — have not been reported. In this report, we address the functional roles and mechanisms by which MIF regulates renal cyst epithelial cell proliferation and apoptosis, glucose uptake and ATP production, macrophage recruitment and retention to pericystic/interstitial sites in mice with cystic kidneys, the interplay among downstream signaling pathways related to PKD, and the extent to which KO of *Mif* or MIF inhibitor slows cyst expansion.

Results

MIF expression was upregulated in Pkd1 mutant renal epithelial cells and tissues, as well as in ADPKD kidneys. To determine if MIF plays a role in PKD and regulates PKD-relevant signaling pathways, we investigated the expression of MIF in *Pkd1* mutant renal epithelial cells and tissues, as well as in ADPKD kidneys. We found that MIF expression was increased in *Pkd1* mutant mouse embryonic kidney (MEK) cells and postnatal *Pkd1* homozygous PN24 cells compared with *Pkd1* WT MEK cells and postnatal *Pkd1* heterozygous PH2 cells, as analyzed with Western blot (Figure 1A) and quantitative reverse transcription PCR (qRT-PCR) (Figure 1B). The expression of MIF was also upregulated in kidneys or in cyst-lining epithelia in kidneys from *Pkd1^{fl/fl} Ksp-Cre m*ice or *Pkd1^{fl/fl} Pkhd1-Cre* mice compared with age-matched controls, as analyzed with qRT-PCR (Figure 1C) and immunohistochemistry staining (Figure 1, D and E). Similar elevation of MIF was observed in human kidney cysts obtained from ADPKD patients (Figure 1F). We further found that MIF was detected in the fractions of plasma membrane and cytosol but not in the nuclear fraction of the cystic renal epithelial cells, as shown by cell fraction-
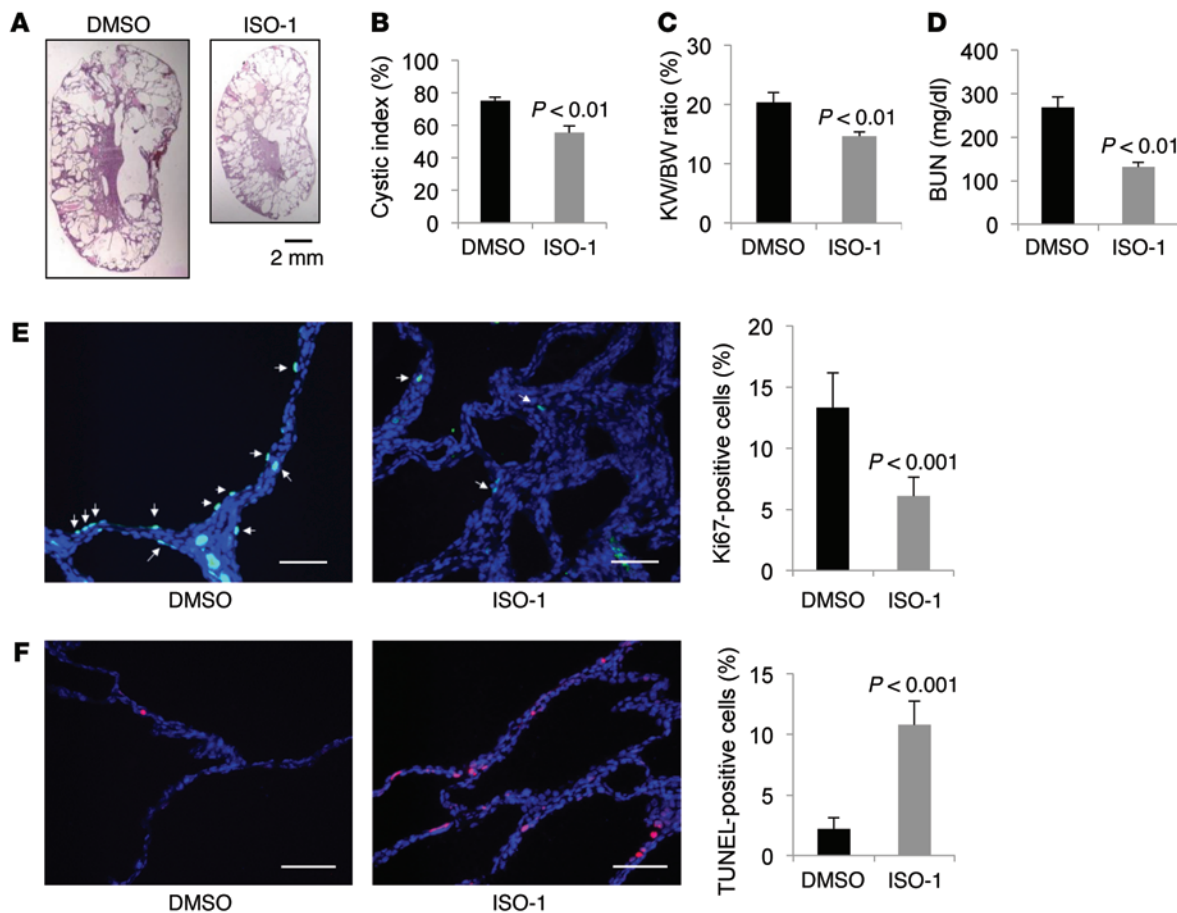
Figure 2. Treatment with ISO-1 delayed cyst growth in *Pkd1^{fl/fl} Pkhd1-Cre* mice. (**A**) Histologic examination of PN25 kidneys from *Pkd1^{fl/fl} Pkhd1-Cre* mice treated with vehicle (DMSO) (*n* = 10) or ISO-1 (*n* = 10). Scale bar: 2 mm. (**B**) Quantification of the percentage of cystic areas over total kidney-section areas of PN25 kidney sections from *Pkd1^{fl/fl} Pkhd1-Cre* mice treated as in **A**. Shown is mean ± SEM of all sections quantified for each condition. *P* < 0.01. (**C** and **D**) KW/BW ratios (**C**) and BUN levels (**D**) were decreased in *Pkd1^{fl/fl} Pkhd1-Cre* mice at PN25 treated with ISO-1 compared with mice treated with DMSO (control). *P* < 0.01. (**E**) ISO-1 treatment reduced cyst-lining epithelial cell proliferation in *Pkd1^{fl/fl} Pkhd1-Cre* mouse kidneys at PN25 as detected by Ki67 staining. *P* < 0.001. Scale bars: 100 μm. Arrows indicate Ki67-positive cells. (**F**) ISO-1 treatment induced cyst-lining epithelial cell apoptosis in *Pkd1^{fl/fl} Pkhd1-Cre* mouse kidneys at PN25 as detected by TUNEL assay. *P* < 0.001. Scale bars: 100 μm. Statistical analysis was performed using an unpaired 2-tailed Student's *t* test.

ation analysis (Supplemental Figure 1; supplemental material available online with this article; doi:10.1172/JCI80467DS1). These results suggest that the increased expression of MIF is due to the loss or mutation of *Pkd1* in renal epithelial cells and tissues.

An inhibitor of MIF, isoxazolines (ISO-1), delays cyst growth in Pkd1 mutant kidneys. Given the robust evidence of upregulation of MIF in cystic renal epithelial cells and tissues, it is reasonable to investigate whether targeting MIF with its inhibitor delayed cyst growth in vivo. Current therapeutic strategies for targeting MIF focus on inhibiting its tautomerase activity by small molecules, including ISO-1, which acts by competing with the substrate for the catalytic site (36). We first tested whether inhibiting the activity of MIF with ISO-1 could reduce cyst growth in a *Pkd1^{fl/fl} Ksp-Cre* mouse model, an aggressive cyst-progression animal model of ADPKD (37). We injected *Pkd1^{fl/fl} Ksp-Cre* pups i.p. with ISO-1 (35 mg/kg) or DMSO daily from postnatal day 3 (PN3) to PN6, and kidneys were harvested and analyzed at PN7. We found that administration of ISO-1 (*n* = 6) delayed cyst growth characterized by partial preservation of renal parenchyma (Supplemental Figure 2A) and a significant decrease in cystic index

(Supplemental Figure 2B) and the kidney weight/body weight ratios (KW/BW ratios) (Supplemental Figure 2C) in the *Pkd1^{fl/fl} Ksp-Cre* mice compared with DMSO-injected *Pkd1^{fl/fl} Ksp-Cre* mice, whereas ISO treatment had no effect on the body weight of these mice (Supplemental Figure 3A). Reduction in cyst growth correlated with significantly improved renal function, as indicated by lower blood urea nitrogen (BUN) levels in ISO-1–treated mice (Supplemental Figure 2D). In addition, the proliferation of the cystic-lining epithelial cells, as analyzed by Ki67 staining (Supplemental Figure 2E), was significantly decreased, but the apoptosis of the cyst-lining epithelia as analyzed by TUNEL assay, was significantly induced (Supplemental Figure 2F) in ISO-1–treated kidneys of *Pkd1^{fl/fl} Ksp-Cre* mice compared with the DMSO-treated mice.

Next, we determined if ISO-1 reduced cyst growth in *Pkd1^{fl/fl} Pkhd1-Cre* mice, a milder *Pkd1* conditional KO mouse model. The cyst growth in *Pkd1^{fl/fl} Pkhd1-Cre* mice begins around PN10, followed by rapid cyst development over the subsequent 2 weeks (6). We treated *Pkd1^{fl/fl} Pkhd1-Cre* pups with daily i.p. injection of ISO-1 (35 mg/kg) or DMSO (control) from PN8–PN24. The kidneys
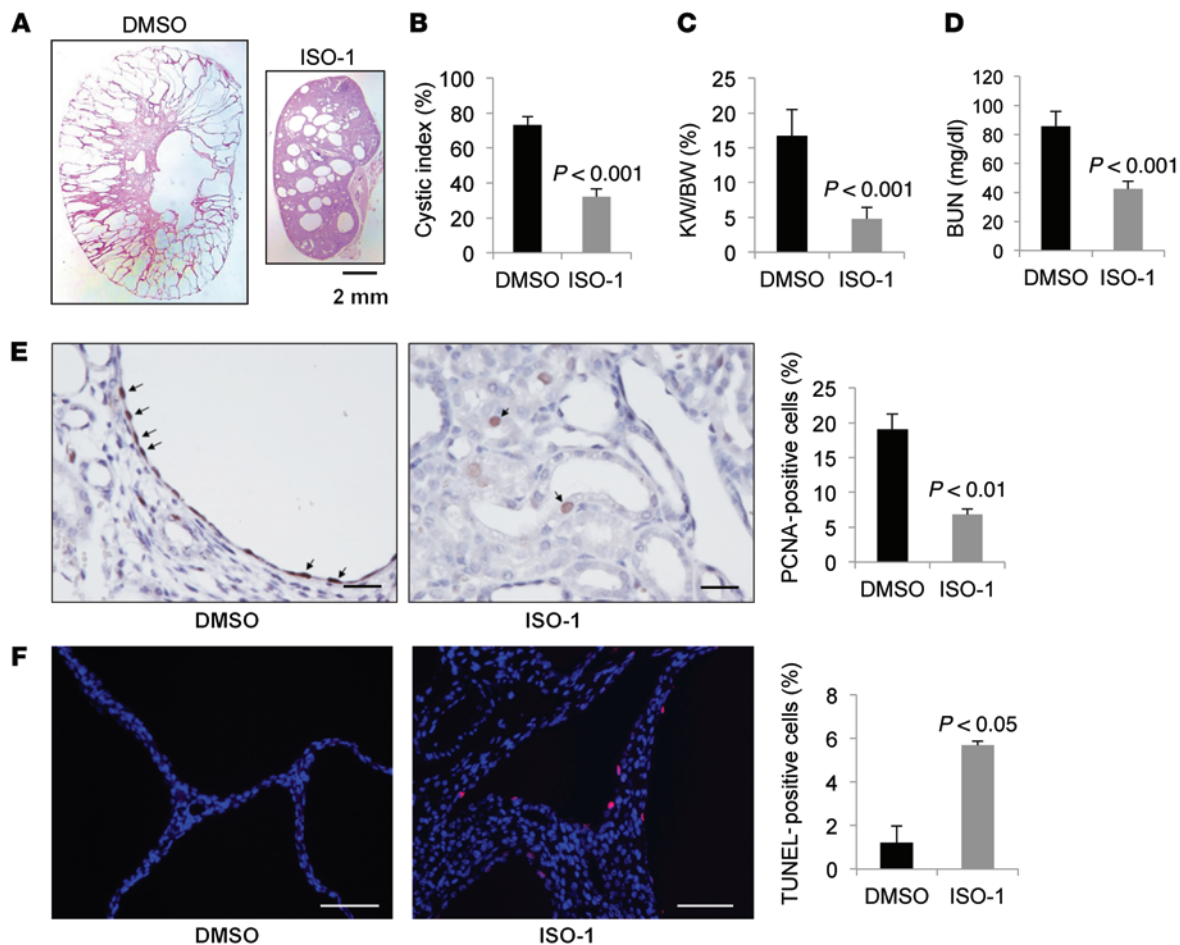
Figure 3. Treatment with ISO-1 delayed cyst growth in *Pkd1*^nl/nl mice. (A) Histologic examination of PN28 kidneys from *Pkd1*^nl/nl mice treated with vehicle (DMSO) (*n* = 12) or ISO-1 (*n* = 6). Scale bar: 2 mm. **(B)** Quantification of the percentage of cystic areas over total kidney-section areas of PN28 kidney sections from *Pkd1*^nl/nl mice treated as in **A**. Shown is mean ± SEM of all sections quantified for each condition. *P* < 0.001. **(C** and **D)** KW/BW ratios **(C)** and BUN levels **(D)** were decreased in *Pkd1*^nl/nl mice at PN28 treated with ISO-1 compared with mice treated with DMSO (control). *P* < 0.001. **(E)** ISO-1 treatment reduced cyst-lining epithelial cell proliferation in *Pkd1*^nl/nl mouse kidneys at PN28, as detected by PCNA staining. Arrows indicate PCNA-positive cells. *P* < 0.01. Scale bars: 50 μm. **(F)** ISO-1 treatment induced cyst-lining epithelial cell apoptosis in *Pkd1*^nl/nl mouse kidneys at PN28 as detected by TUNEL assay. *P* < 0.05. Scale bars: 100 μm. Statistical analysis was performed using an unpaired 2-tailed Student's *t* test.

were harvested and analyzed at PN25, and we found that ISO-1 treatment did not affect the body weight, compared with DMSO-treated mice (Supplemental Figure 3B). However, administration of ISO-1 (*n* = 10) delayed renal cyst growth (Figure 2A) characterized by significantly decreasing cyst index (Figure 2B), the KW/BW ratios (Figure 2C), and BUN levels (Figure 2D), as well as by inhibiting cystic epithelial cell proliferation, as analyzed with Ki67 staining (Figure 2E), and inducing cyst-lining epithelial cell apoptosis, as analyzed with TUNEL assay (Figure 2F), in kidneys from *Pkd1*^fl/fl *Pkhd1-Cre* mice compared with the age-matched kidneys from DMSO-injected *Pkd1*^fl/fl *Pkhd1-Cre* mice (*n* = 10).

Last, we determined if ISO-1 reduced cyst growth in *Pkd1*^nl/nl mice, a milder *Pkd1* hypomorphic mouse model (38). We treated *Pkd1*^nl/nl pups with daily i.p. injection of ISO-1 (35 mg/kg) or DMSO (control) from PN5–PN27. The kidneys were harvested and analyzed at PN28, and we also found that ISO-1 treatment did not affect the body weight compared with DMSO-treated mice (Supplemental Figure 3C). However, administration of ISO-1 (*n* = 6) delayed renal cyst growth (Figure 3A), characterized by significantly

decreasing cyst index (Figure 3B, *P* < 0.001), the KW/BW ratios (Figure 3C, *P* < 0.001), and BUN levels (Figure 3D, *P* < 0.001), as well as by inhibiting cystic epithelial cell proliferation as analyzed with proliferating cell nuclear antigen (PCNA) staining (Figure 3E) and inducing cyst-lining epithelial cell apoptosis as analyzed with TUNEL assay (Figure 3F) in kidneys from *Pkd1*^nl/nl mice compared with that in the age-matched kidneys from DMSO-injected *Pkd1*^nl/nl mice (*n* = 12). These results suggest that targeting MIF with pharmacological inhibitors may delay cyst growth in ADPKD patients.

MIF and Pkd1 double KO delays renal cyst growth. To further explore the in vivo function of MIF in a *Pkd1* KO mouse model, we crossed the *Pkd1*^fl/+ *Ksp-Cre Mif*^+/− female mice with *Pkd1*^fl/+ *Ksp-Cre Mif*^+/− male mice to generate *Pkd1*^fl/fl *Ksp-Cre Mif*^−/− mice. We found that cyst formation was significantly delayed in the absence of MIF in *Pkd1*^fl/fl *Ksp-Cre Mif*^−/− mice (*n* = 6) at PN7 compared with age-matched *Pkd1*^fl/fl *Ksp-Cre Mif*^+/+ mice (*n* = 10) (Figure 4, A and B). The KW/BW ratios from *Pkd1*^fl/fl *Ksp-Cre Mif*^−/− mice were dramatically reduced compared with *Pkd1*^fl/fl *Ksp-Cre Mif*^+/+ mice (Figure 4C). In addition, BUN levels were also significantly reduced in *Pkd1*^fl/fl *Ksp-Cre Mif*^−/−
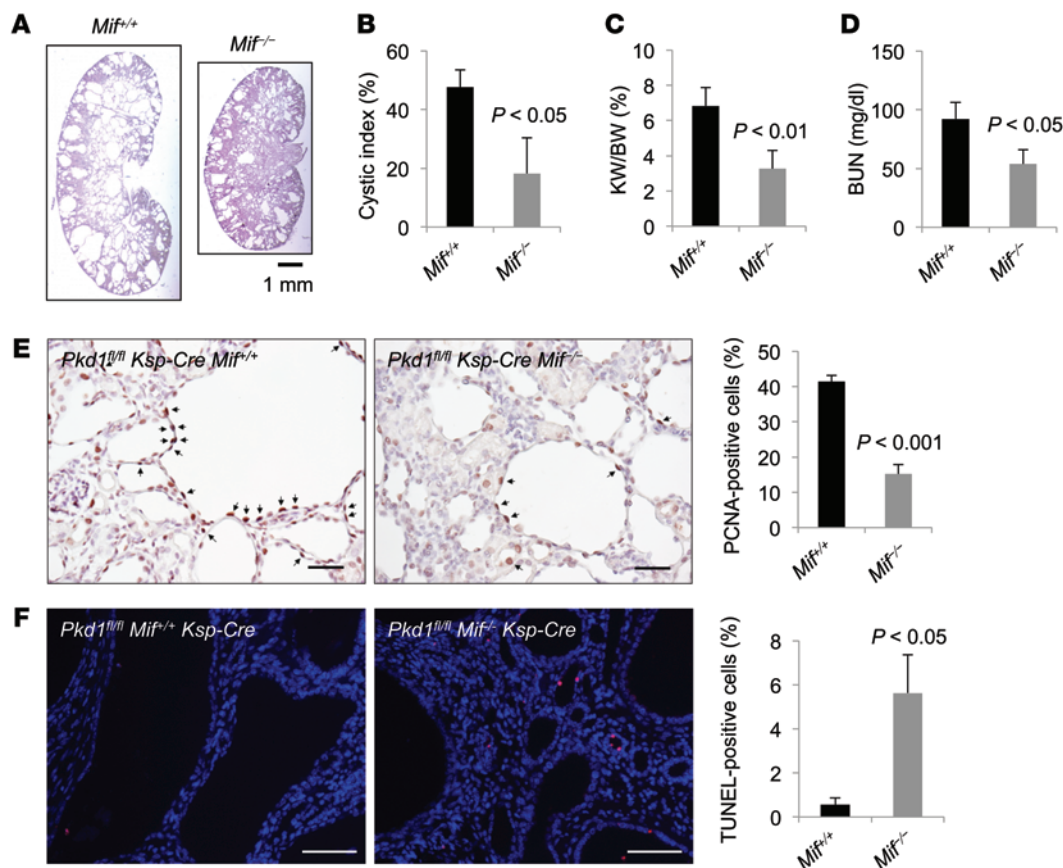
Figure 4. MIF and *Pkd1* double KO delayed renal cyst formation. (**A**) Histologic examination of PN7 kidneys from *Pkd1*$^{fl/fl}$ *Ksp-Cre Mif*$^{+/+}$ (*Mif*$^{+/+}$) and *Pkd1*$^{fl/}$ ^{fl} *Ksp-Cre Mif*$^{-/-}$ (*Mif*$^{-/-}$) neonates. Scale bar: 1 mm. (**B**) Cystic index was significantly decreased in PN7 kidneys from *Mif*$^{-/-}$ neonates (n = 6) compared with *Mif*$^{+/+}$ neonates (n = 10) ($P < 0.05$). Shown is mean ± SEM of all sections quantified for each condition. (**C**) KW/BW ratios from PN7 *Mif*$^{-/-}$ neonates were dramatically reduced compared with PN7 *Mif*$^{+/+}$ neonates. Shown is mean ± SEM. $P < 0.05$. (**D**) BUN levels of PN7 *Mif*$^{+/+}$ and *Mif*$^{-/-}$ neonates. Shown is mean ± SEM. $P < 0.05$. (**E**) Cell proliferation was decreased in *Mif*$^{-/-}$ neonate kidneys compared with *Mif*$^{+/+}$ kidneys, as detected with PCNA staining. On average, the percentage of PCNA-positive nuclei in cyst-lining epithelial cells was calculated from 1,000 nuclei per mouse-kidney section, and only strongly stained nuclei were considered as PCNA-positive. Shown is mean ± SEM. $P < 0.001$. Scale bars: 50 μm. Arrows indicate the PCNA-positive cells. (**F**) KO of *Mif* induced cyst-lining epithelial cell apoptosis in *Pkd1*$^{fl/fl}$ *Ksp-Cre* mouse kidneys, as detected by TUNEL assay. $P < 0.05$. Scale bars: 100 μm. Statistical analysis was performed using an unpaired 2-tailed Student's *t* test.

mice compared with *Pkd1*$^{fl/fl}$ *Ksp-Cre Mif*$^{+/+}$ mice, which indicated that renal function was normalized in *Pkd1*$^{fl/fl}$ *Ksp-Cre Mif*$^{-/-}$ mice (Figure 4D). At the same time, the expression of MIF could not be detected in kidneys from *Pkd1* and *Mif* double KO mice, as analyzed by Western blot (Supplemental Figure 4). PCNA staining revealed that the proliferation of cyst-lining epithelial cells was significantly decreased in *Pkd1* and *Mif* double KO renal epithelia compared with *Pkd1* conditional KO and WT *Mif* (Figure 4E), whereas TUNEL staining showed that KO of *Mif* induced apoptosis in *Pkd1* conditional KO kidneys (Figure 4F).

ISO-1 treatment reduces macrophages at interstitial and pericystic regions in Pkd1 conditional KO mouse kidneys. It has been reported that large numbers of renal macrophages are recruited to interstitial and pericystic regions in orthologous models of *PKD1*, *PKD2*, and *cpk* mice (5, 6), and that an abundance of M2-like macrophages promotes cystic renal cell proliferation and cyst growth (5). We found that double KO of *Pkd1* and *Mif* decreased the accumulation/recruitment of macrophages to pericystic sites and interstitium in kidneys compared with kidneys from *Pkd1* single KO *Pkd1*$^{fl/}$ ^{fl} *Ksp-Cre* mice (Supplemental Figure 5A). We also found that in

addition to decreasing cell proliferation and inducing apoptosis in cyst-lining epithelia in vivo, treatment with ISO-1 also dramatically reduced the accumulation/recruitment of macrophages to pericystic sites and interstitium in kidneys from *Pkd1*$^{fl/fl}$ *Ksp-Cre* mice and *Pkd1*$^{fl/fl}$ *Pkhd1-Cre* mice compared with DMSO-treated *Pkd1*$^{fl/fl}$ *Ksp-Cre* mice and *Pkd1*$^{fl/fl}$ *Pkhd1-Cre* mice (Supplemental Figure 5, B–D). ISO-1 was reported to inhibit the tautomerase activity of MIF by competing with the substrate for the catalytic site (36). However, we found that ISO-1 treatment also decreased the levels of MIF in kidneys from *Pkd1*$^{fl/fl}$ *Ksp-Cre* mice and *Pkd1*$^{fl/fl}$ *Pkhd1-Cre* mice, as determined by Western blot (Supplemental Figure 6, A and B) and immunohistochemistry staining (Supplemental Figure 6, C and D). These results suggest a role of MIF in regulating the recruitment of macrophages to pericystic sites and interstitium of ADPKD.

MIF can be secreted into cell-culture mediums of renal epithelial cells and is highly enriched in cyst fluids and urines derived from 2 distinct orthologous mouse models of ADPKD. The proliferative effect of macrophages on cyst growth does not require cell-cell contact but can be mediated via unknown soluble factors (5). Western blot analysis of conditioned media showed that renal epithelial cells can
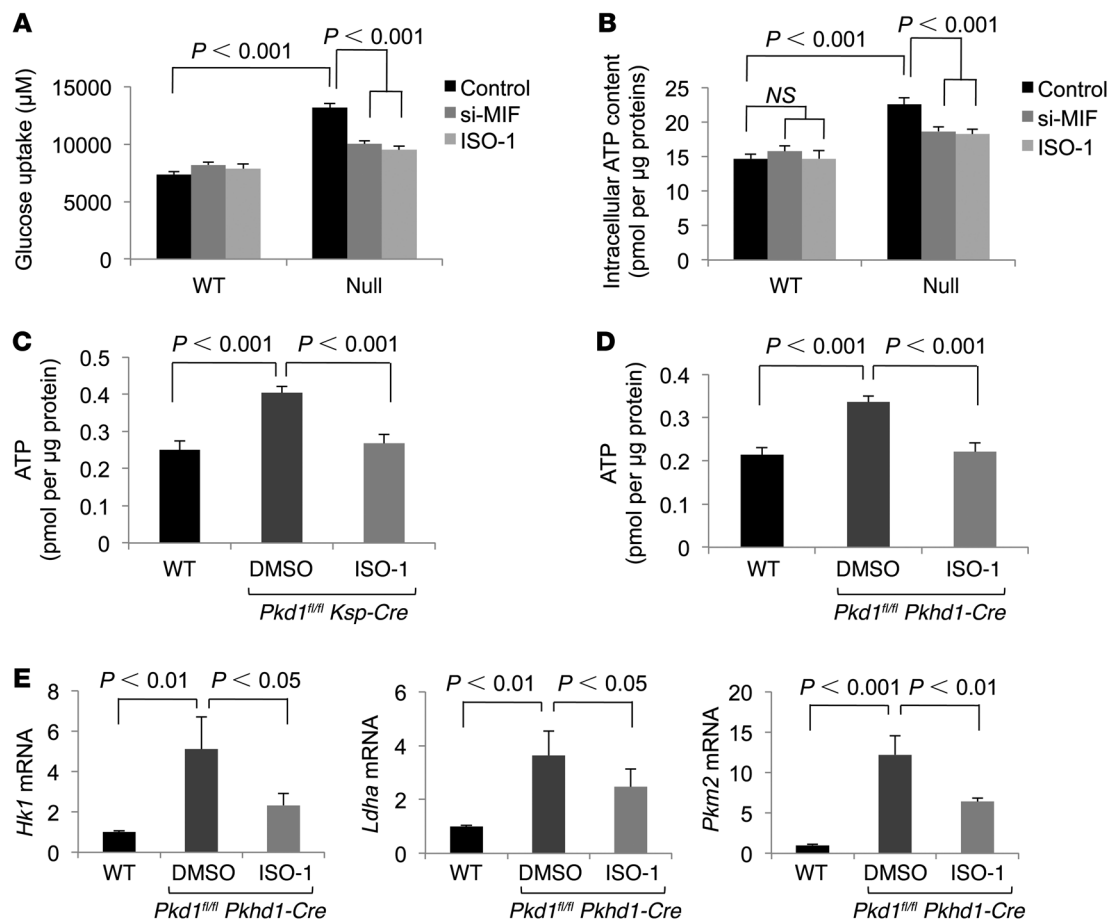
Figure 5. MIF promotes glucose uptake and ATP generation in renal epithelial cells and tissues. (**A**) Knockdown of MIF with siRNA or inhibition of MIF with ISO-1 decreased the uptake of glucose in *Pkd1* mutant MEK cells compared with untreated *Pkd1* mutant MEK cells. n = 3, $P < 0.001$; ANOVA post hoc test. (**B**) Knockdown of MIF with siRNA or inhibition of MIF with ISO-1 decreased the levels of intracellular ATP in *Pkd1* mutant MEK cells compared with untreated *Pkd1* mutant MEK cells. n = 3, $P < 0.001$; ANOVA post hoc test. (**C** and **D**) Treatment with ISO-1 decreased the levels of intracellular ATP in kidneys from *Pkd1*^fl/fl *Ksp-Cre* mice at PN7 (**C**) and from *Pkd1*^fl/fl *Pkhd1-Cre* mice at PN25 (**D**). n = 5, $P < 0.001$; ANOVA post hoc test. (**E**) qRT-PCR analysis of the expression of *Hk1*, *Ldha*, and *Pkm2* mRNA in PN25 kidneys from *Pkd1*^fl/fl *Pkhd1-Cre* mice treated with ISO-1 or DMSO. n = 3, $P < 0.05$; ANOVA post hoc test. The mRNA levels of these genes were normalized to mRNA levels in WT kidneys, which is set as 1.

secrete MIF, and *Pkd1* mutant renal epithelial cells secreted more MIF than *Pkd1* WT renal epithelial cells when MIF levels were normalized to cell number (Supplemental Figure 7A). Moreover, MIF was highly enriched in cyst fluid collected from *Pkd1*^fl/fl *Ksp-Cre* mice and *Pkd1*^fl/fl *Pkhd1-Cre* mice (Supplemental Figure 7B). MIF was only detected in urine from *Pkd1*^fl/fl *Ksp-Cre* mice and *Pkd1*^fl/fl *Pkhd1-Cre* mice, but not from age-matched *Pkd1* WT mice (Supplemental Figure 7C). Furthermore, MIF was detected in cyst fluids from ADPKD patients (Supplemental Figure 8A) and in the urine of ADPKD patients (Supplemental Figure 8B). The MIF levels in the urines of normal volunteers were very low, as shown by weak bands in some samples (Supplemental Figure 8B). These results suggested that MIF in cyst fluids and urines might be secreted by renal epithelial cells and/or macrophages accumulated in pericystic sites and interstitium of kidneys in *Pkd1* KO mice and ADPKD patients, and MIF might work as a soluble mediator to regulate intracellular signaling pathways through its receptors.

MIF is a soluble factor secreted by ADPKD cells into ADPKD-conditioned medium and promotes macrophage migration and the expression of MCP-1 and TNF-α. To investigate whether MIF

present in ADPKD conditioned medium (CM) may contribute to macrophage recruitment in our established system as described (5), we tested the effects of ISO-1 on the monocyte chemoattractant activity present in this CM. For these experiments, transwell migration assays of THP-1 cells, a human monocyte cell line, were carried out. We found that while ADPKD CM promoted robust migration of monocytes, this effect was significantly diminished by the presence of ISO-1 (Supplemental Figure 9). These results support that MIF, as a factor secreted by ADPKD cells, promotes the migration of macrophages.

Accumulation of macrophages was associated with the increased expression of MCP-1 in the kidneys of Han:SPRD polycystic rats, a nonorthologous model of ADPKD (39). We found, by Western blot analysis, that the expression of MCP-1 was elevated in *Pkd1* mutant renal epithelial cells (Supplemental Figure 10A). We found similar results by immunohistochemistry staining in cyst-lining epithelia in kidneys from *Pkd1*^fl/fl *Ksp-Cre* mice and *Pkd1*^fl/fl *Pkhd1-Cre* mice, as well as in kidneys from ADPKD patients (Supplemental Figure 10, B–D). Treatment with ISO-1 decreased the expression of MCP-1 in *Pkd1* mutant kidneys from *Pkd1*^fl/fl *Ksp-*
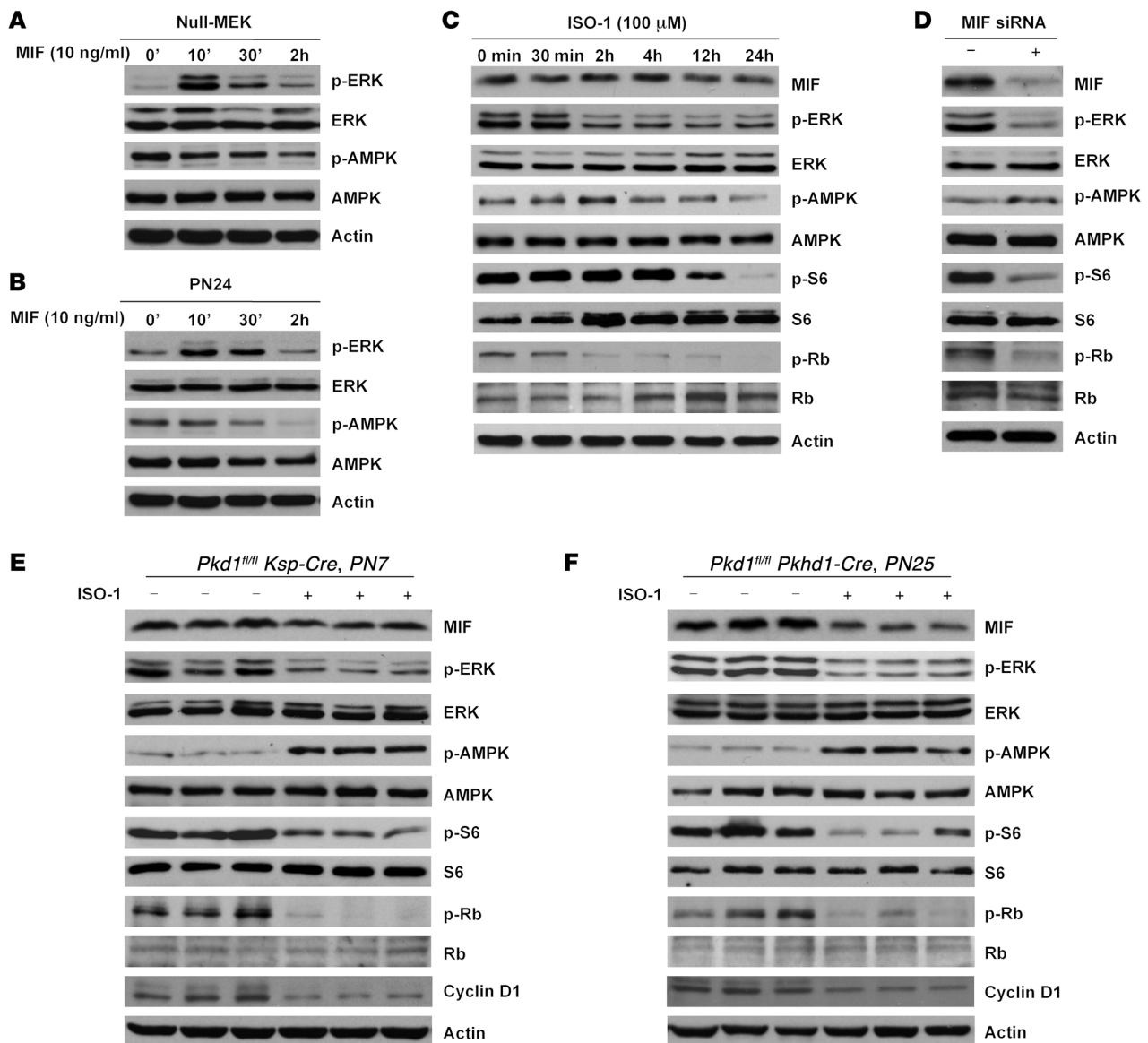
Figure 6. MIF regulates renal epithelial cell proliferation through activation of ERK, mTOR, and Rb/E2F signaling pathways. (**A** and **B**) Western blot analysis of the expression of ERK and phospho-ERK, as well as AMPK and phospho-AMPK, from whole-cell lysates of *Pkd1* null MEK (Null-MEK) cells (**A**) and *Pkd1* mutant PN24 cells (**B**) induced with MIF (10 ng/ml) at indicated time points. (**C**) Western blot analysis of the expression of ERK and phospho-ERK, AMPK and phospho-AMPK, S6 and phospho-S6, and Rb and phospho-Rb from whole-cell lysates of *Pkd1* mutant PN24 cells treated with ISO-1 (100 μM) at indicated time points. (**D**) Western blot analysis of the expression of ERK and phospho-ERK, AMPK and phospho-AMPK, S6 and phospho-S6, and Rb and phospho-Rb from whole-cell lysates of *Pkd1* mutant PN24 cells transfected with MIF siRNA or control siRNA. (**E** and **F**) Western blot analysis of the expression of ERK and phospho-ERK, AMPK and phospho-AMPK, S6 and phospho-S6, and Rb and phospho-Rb in kidneys from 3 different *Pkd1^fl/fl* *Ksp-Cre* mice (**E**) and *Pkd1^fl/fl* *Pkhd1-Cre* mice (**F**) treated with DMSO or ISO-1.

Cre mice (Supplemental Figure 10B) and *Pkd1^fl/fl Pkhd1-Cre* mice (Supplemental Figure 10C) compared with age-matched control kidneys treated with DMSO. In addition, we found that treatment with ISO-1 decreased the levels of MCP-1 mRNA and protein in kidneys from *Pkd1^fl/fl Pkhd1-Cre* mice compared with DMSO-treated control (Supplemental Figure 11). We also found that MIF induced the expression of MCP-1 and TNF-α in *Pkd1* mutant renal epithelial cells (Supplemental Figure 12, A and B), whereas TNF-α also induced the expression of MIF in renal epithelial cells (Supplemental Figure 12C). It has been reported that MIF induces macrophage recruitment through chemokine CCL2 (MCP-1) (26).

Our results suggested that MIF is an upstream regulator of MCP-1 and may regulate MCP-1–mediated recruitment/retention of macrophages to the kidneys of ADPKD patients.

MIF promotes glucose uptake and ATP generation in cystic renal epithelial cells and tissues. MIF has been reported to regulate glucose uptake in non–small cell lung carcinomas (23) and to stimulate glycolysis during sepsis (40). Deprivation of glucose abrogated the higher ATP content of *Pkd1* mutant mouse embryonic fibroblasts (MEFs), and glucose addition increased the intracellular ATP in these cells (33). We found glucose uptake and ATP levels were elevated in *Pkd1* mutant (Null) MEK cells compared with *Pkd1* WT
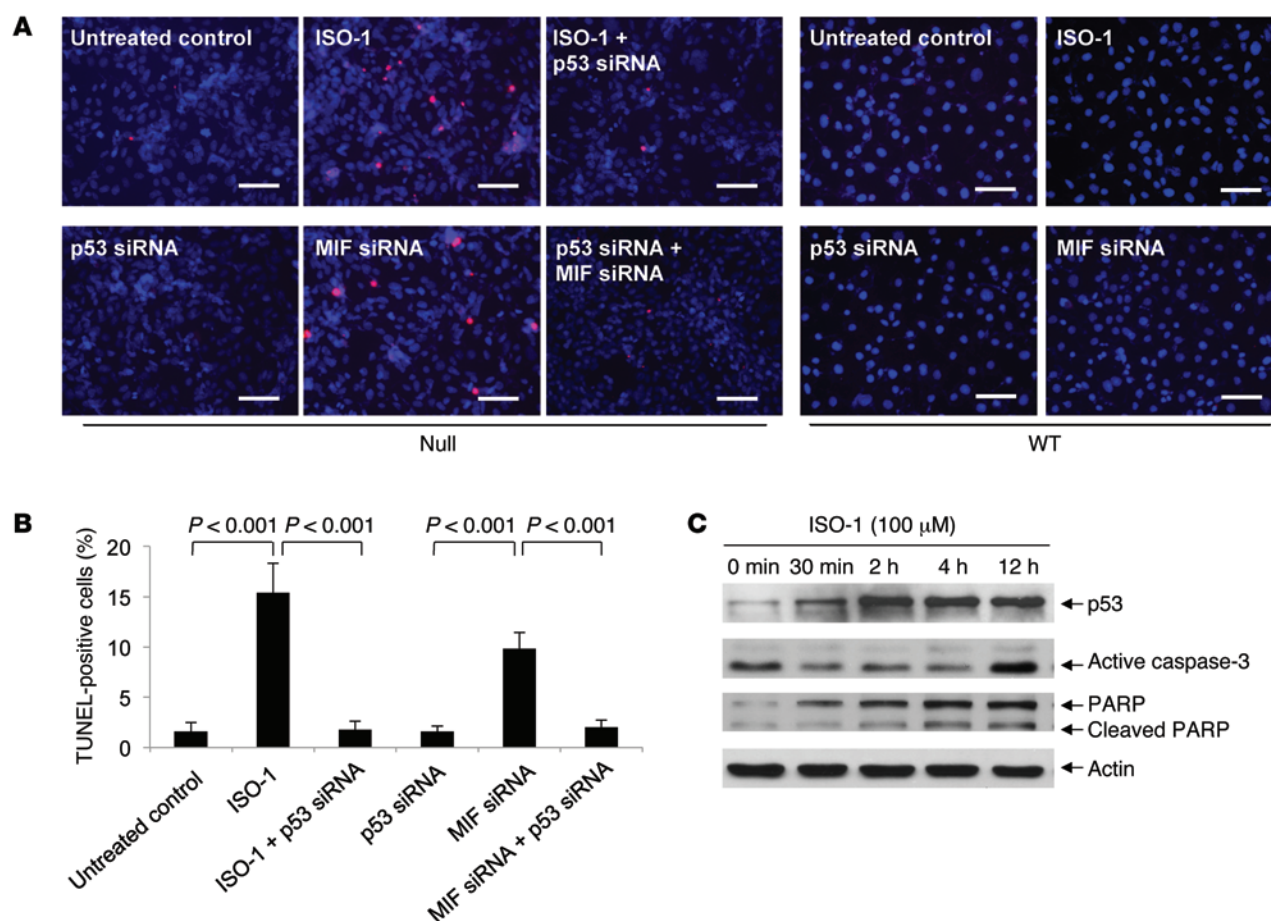
Figure 7. MIF regulates cystic epithelial survival and death via p53. (**A** and **B**) Inhibition of MIF with ISO-1 or knockdown of MIF with siRNA-induced apoptosis in *Pkd1* null MEK cells (**A**, left panel) while knockdown of p53 with siRNA prevented ISO-1– or MIF siRNA–induced apoptosis in these cells as detected by TUNEL assay, which were transfected with p53 siRNA for 24 hours and then treated with 100 μM ISO-1 or MIF siRNA for 24 hours. *P* < 0.001; ANOVA post hoc test. However, inhibition of MIF with ISO-1 or knockdown of MIF with siRNA did not induce apoptosis in *Pkd1* WT MEK cells (**A**, right panel). Scale bar: 100 μm. (**C**) Western blot analysis of the expression of p53 and active caspase-3, as well as the cleaved poly (ADP-ribose) polymerase (PARP), a substrate of caspase-3 in *Pkd1* null MEK cells treated with ISO-1 (100 μM) at indicated time points. The expression of p53 and active caspase-3, as well as the cleaved PARP, were gradually increased in *Pkd1* null MEK cells treated with ISO-1 up to 12 hours, compared with untreated cells (0 hour).

MEK cells (Figure 5, A and B). Treatment with ISO-1 or knockdown of MIF with siRNA decreased the uptake of glucose (Figure 5A) and the levels of intracellular ATP in *Pkd1* mutant renal epithelial cells (Figure 5B), but it had no significant effects on those in *Pkd1* WT MEK cells (Figure 5, A and B). Consistent with a switch to glycolysis, treatment with ISO-1 decreased the transcription of the key glycolytic enzymes, *Hk1* and *Ldha*, in *Pkd1* mutant renal epithelial cells (Supplemental Figure 13).

We also investigated whether MIF affected the glycolysis and ATP generation in vivo. Levels of ATP (Figure 5, C and D) and mRNA expression of key glycolytic enzymes *Hk1*, *Ldha*, and *Pkm2* (Figure 5E) in kidneys from *Pkd1*^fl/fl^ *Ksp-Cre* mice and *Pkd1*^fl/fl^ *Pkhd1-Cre* mice were increased, compared with age-matched WT mice. We found that ISO-1 treatment decreased the levels of ATP in kidneys from *Pkd1*^fl/fl^ *Ksp-Cre* mice (Figure 5C) and *Pkd1*^fl/fl^ *Pkhd1-Cre* mice (Figure 5D), as compared with kidneys from DMSO-injected *Pkd1*^fl/fl^ *Ksp-Cre* mice and *Pkd1*^fl/fl^ *Pkhd1-Cre* mice; this was similar to those observed in vitro. And the transcription of *Hk1*, *Ldha*, and *Pkm2* was also decreased in kidneys from ISO-1–treated *Pkd1*^fl/fl^

Pkhd1-Cre mice, compared with DMSO-treated *Pkd1*^fl/fl^ *Pkhd1-Cre* mice (Figure 5E). Our results suggested that MIF regulated glucose uptake and ATP levels in renal epithelial cells and tissues.

MIF regulates renal epithelial cell proliferation through activation of ERK, mTOR, and Rb/E2F signaling pathways. MIF, as a pleiotropic proinflammatory cytokine, regulates not only the recruitment of innate and adaptive immune cells to the place of inflammation, but also cell proliferation, cell differentiation, and apoptosis (41), which are the drivers of cyst growth (2, 4), thus suggesting that multiple MIF-mediated mechanisms and signaling pathways are likely to be involved in MIF-mediated cyst growth. MIF exerts its biological activities through signal transduction, initiated by direct binding to the CD74/CD44 receptor complex to activate the downstream signaling pathways (42). MIF binds to CD74, a type II transmembrane protein, inducing its phosphorylation and the recruitment of CD44, which then activates SRC tyrosine kinases, leading to phosphorylation of ERK1/2 and the further activation of downstream effector proteins involved in inflammatory processes and cell proliferation (20, 21). We found that MIF induced rapid
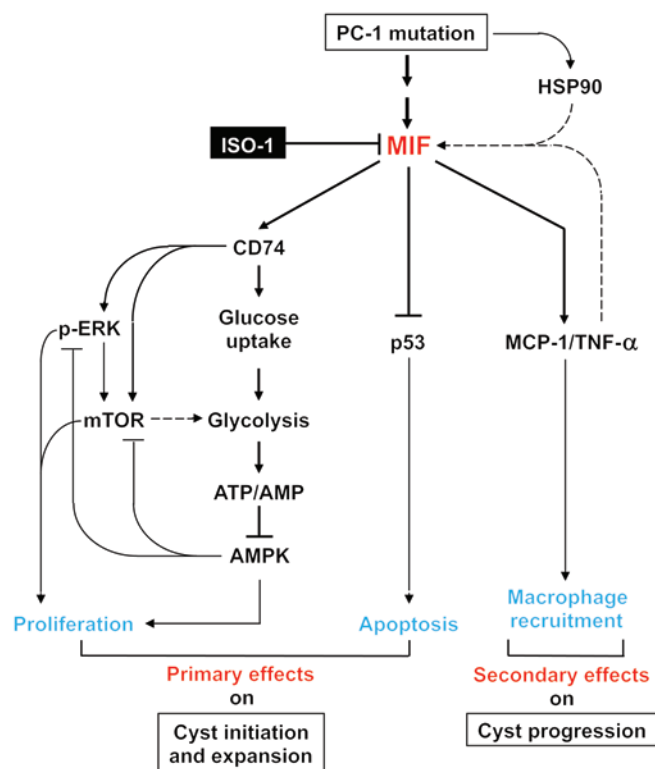
Figure 8. A schematic diagram depicting MIF-mediated pathways and processes in *Pkd1* mutant renal epithelial cells. *Pkd1* KO or mutation results in the upregulation of MIF, which may be stabilized via HSP90, induced by cyst fluid TNF-α or through another unknown mechanism. Upregulated MIF in *Pkd1* mutant renal epithelial cells activates ERK and mTOR signaling, which may result in activation of ERK-mTOR–mediated cell proliferation and glycolysis, as has been suggested. It also increases glucose uptake, which results in promoting glycolysis and the generation of ATP to inhibit AMPK; inhibits p53-dependent cystic epithelial cell death; is responsible for the recruitment of macrophages to pericystic and interstitial regions in *Pkd1* mutant mouse kidneys, a process likely to be enhanced by MIF-mediated upregulation of MCP-1 and/or TNF-α; and is a target of ISO-1, which delays cyst growth in *Pkd1* KO mouse kidneys. In addition, 2 double-negative feedback loops downstream of MIF can be observed: among ERK-mTOR-glycolysis-AMPK-ERK and among mTOR-gly-colysis-AMPK-mTOR. Arrow indicates the positive effect; "T" indicates the negative effect. Dashed lines indicate putative signaling mechanisms.

and transient activation of ERK — a canonical PKD1 effector (33, 35) — in *Pkd1* mutant renal epithelial cells at 10 minutes (Figure 6, A and B), while inhibition of MIF with ISO-1 or knockdown MIF with siRNA decreased the phosphorylation and activation of ERK in these cells (Figure 6, C and D, and Supplemental Figure 14A). To support that MIF as a soluble factor that is able to induce the phosphorylation of ERK, we found that CM collected from MIF knockdown cystic renal epithelial cells did not stimulate the phosphorylation of ERK in *Pkd1* null cells and PN24 cells, whereas the CM collected from control siRNA transfected cells did induce the phosphorylation of ERK in these cells (Supplemental Figure 14B). This observation was confirmed in vivo; targeting MIF with ISO-1 decreased the phosphorylation of ERK in kidneys from *Pkd1*^{fl/fl} *Ksp-Cre* mice (Figure 6E) and *Pkd1*^{fl/fl} *Pkhd1-Cre* mice (Figure 6F) as compared with kidneys from DMSO-injected *Pkd1*^{fl/fl} *Ksp-Cre* mice and *Pkd1*^{fl/fl} *Pkhd1-Cre* mice (Figure 6, E and F).

Next, we found that endogenous MIF is necessary for the phosphorylation of S6, a substrate of mTOR complex 1, in *Pkd1* mutant renal epithelial cells. As shown in Figure 6, C and D, inhibition of MIF with ISO-1 or knockdown MIF with siRNA resulted in a pronounced reduction of phosphorylation of S6 in *Pkd1* mutant renal epithelial cells, which indicated that MIF was an upstream regulator of mTOR signaling in those cells. It has been reported that mTOR activity can be inhibited by activated AMPK that accompanies metabolic stress induction by glucose restriction (23). Correspondingly, decreases in glucose uptake (Figure 5A) and S6 phosphorylation were commensurate with increases in the phosphorylation of AMPK in *Pkd1* mutant renal epithelial cells upon treatment with ISO-1 or MIF siRNA (Figure 6, C and D). We

further found that treatment with ISO-1 decreased the activation and phosphorylation of S6 (Figure 6, E and F) but sustained activation of AMPK in *Pkd1* mutant kidneys (Figure 6, E and F). These results suggest that MIF regulates the interplay between mTOR and AMPK signaling in regulating *Pkd1* mutant renal epithelial cell proliferation, and this process involves MIF-mediated glucose uptake and ATP production.

MIF has been reported to interfere with the Rb/E2F pathway (28), which was recently shown to regulate cystic renal epithelial cell proliferation (2, 3). We found that inhibition of MIF with ISO-1 or knockdown of MIF with siRNA decreased the phosphorylation of Rb in *Pkd1* mutant renal epithelial cells (Figure 6, C and D) and in *Pkd1* KO kidneys upon ISO-1 treatment (Figure 6, E and F). These results suggested that MIF also affected *Pkd1* mutant renal epithelial cell proliferation through Rb/E2F-dependent mechanisms.

MIF inhibition induces p53-dependent cystic renal epithelial cell apoptosis. Treatment with ISO-1 induced cystic epithelial cell death in *Pkd1* KO renal tissues (Figure 2F, Figure 3F, and Supplemental Figure 1F). Previous studies demonstrated that MIF protects macrophages from p53-mediated apoptosis (24). Thus, we examined whether MIF regulated p53-dependent cystic renal epithelial cell survival and death. We found that inhibition of MIF with ISO-1 or knockdown of MIF with siRNA significantly induced *Pkd1*-null (Null) MEK cell apoptosis (Figure 7, A and B), whereas no apoptotic cells were observed in *Pkd1* WT MEK cells with all these treatments, as analyzed by TUNEL assay (Figure 7A). However, knockdown of p53 with siRNA significantly decreased the apoptosis of *Pkd1* mutant renal epithelial cells induced by inhibi-

tion of MIF with ISO-1 or MIF siRNA–mediated knockdown (Figure 7, A and B), while knockdown of p53 alone had no effect on cell survival and death. The knockdown efficiency of p53 siRNA and MIF siRNA was confirmed by Western blot (data not shown). Treatment with ISO-1 increased the expression of p53 and active caspase-3 in *Pkd1* mutant cystic renal epithelial cells (Figure 7C). Caspase-3 activation was further confirmed by the appearance of cleaved poly (ADP-ribose) polymerase (PARP), a substrate of caspase-3 (Figure 7C).

Discussion

In this study, we provide evidence that MIF is a key regulator of cyst growth in ADPKD and upstream of ERK, AMPK, mTOR, Rb/E2F, and p53 signaling pathways; it is also a regulator of the processes of glucose uptake and macrophage recruitment, and the production of TNF-α and MCP-1. MIF upregulation in renal cyst epithelial cells activates ERK and mTOR signaling, which may result in activation of ERK-mTOR–mediated cell proliferation and glycolysis, as has been suggested (33); increases glucose uptake, which results in promoting glycolysis and production of ATP to increase the ratio of ATP/AMP, which inhibits AMPK; increases the phosphorylation of Rb, which releases E2F from Rb/E2F, thereby increasing S-phase entry; inhibits p53-dependent apoptosis of cyst epithelial cells; and contributes to the recruitment of macrophages to pericystic and interstitial regions in *Pkd1* mutant mouse kidneys, a process possibly regulated by MIF-mediated upregulation of MCP-1 and/or TNF-α (Figure 8). KO of *Mif* or targeting MIF with the inhibitor, ISO-1, delayed cyst growth and improved renal function in *Pkd1* conditional KO mouse models and *Pkd1* hypomorphic mouse model. The treated kidneys were characterized by diminished cyst mural cell proliferation, induced cyst mural cell apoptosis, diminished renal ATP generation, and diminished recruitment of macrophages to the kidneys (Figure 8).

PKD is not primarily an inflammatory disorder; however, recent studies suggest that the chronic interstitial inflammation in PKD contributes to cyst expansion and renal impairment (5, 6). Rather than serving as a primary cause of cyst initiation and expansion, interstitial inflammation secondarily promotes disease progression in response to cyst-initiated macrophage recruitment. Renal cyst growth may involve 2 phases: initiation of cyst formation and progressive cyst enlargement. Initiation is induced by unscheduled proliferation of tubule cells in response to the malfunction of polycystins 1 and 2. As the tubule wall expands and bulges into the interstitium, gene array and proteomic studies have revealed that a large number of secondary processes are set in motion, some of which have deleterious effects. In this regard, the formation of a cyst can be viewed as a microscopic injury to the tubule, provoking an injury response resembling those observed when a wound is created in any organ. In PKD, the lesions never heal and relentlessly enlarge, obstructing the flow of blood, lymph, and urine in nearby vessels (42). Cyst formation induced by genetic mutation of *Pkd1* may set in motion several primary effects, including MIF initiation and regulated activation of ERK, mTOR, and Rb/E2F signaling, leading to increased cyst epithelial cell proliferation; increased glucose uptake and glycolysis that inhibit AMPK signaling; the inhibition of p53 that prevents apoptosis of *Pkd1* mutant renal epithelial cells (Figure 8); and, sec-

ondarily, MIF-mediated recruitment of macrophages in an injury response (43) that promotes cyst expansion and disease progression (Figure 8). By this account, MIF promotes signaling pathways that directly influence cyst initiation and growth of renal epithelial cells, as well as calling to action troublesome inflammatory mediators (Figure 8). The central and upstream position of MIF in the pathogenesis of ADPKD suggests that therapeutically targeting MIF could ameliorate the progression of ADPKD.

MIF regulation in ADPKD. We found that MIF was upregulated in the kidneys of *Pkd1* mutant mice and ADPKD patients (Figure 1). Elevated MIF in ADPKD may be caused by increased transcription due to unknown transcriptional regulators and/or epigenetic regulation, including histone acetylation and methylation, or by protein stabilization due to unknown factors. Our results that TNF-α could induce the expression of MIF in renal epithelial cells (Supplemental Figure 12C) suggested that cyst fluid TNF-α might stimulate the expression of MIF in cyst-lining epithelia in vivo (Figure 8). Together with the result that MIF also stimulates the expression of TNF-α (Supplemental Figure 12A and 12B), a positive feedback loop may exist between MIF and TNF-α in vivo (Figure 8). In addition, HSP90 is upregulated in ADPKD kidneys, and HSP90 inhibition slows cyst growth in a mouse model of ADPKD (44). It has been reported that inhibiting HSP90 destabilizes MIF in breast cancer cells (45), suggesting that the elevated MIF levels in ADPKD may be mediated through HSP90 stabilization (Figure 8). In support of this idea, we found that HSP90 inhibition decreased MIF levels in *Pkd1* mutant renal epithelial cells (Supplemental Figure 15).

MIF and the recruitment of macrophages, as well as the expression/secretion of cytokines. MIF stimulates the expression and secretion of proinflammatory cytokines from macrophages (41). Macrophages secrete TNF-α (46), and increased MCP-1 levels are present in a rat model of PKD (39). Urinary levels of MCP-1 correlate with disease severity, indicating that MCP-1 is a potential biomarker for disease progression (34). Although MIF may be expressed by interstitial T cells and macrophages in the setting of PKD, it is unlikely that macrophages are the only source of cytokines in PKD kidneys. The current results that MIF was secreted by renal epithelial cells into culture medium and cyst fluids (Supplemental Figure 7, A and B); that MCP-1 was elevated in *Pkd1* mutant mouse cells and in mouse and human ADPKD kidneys; that TNF-α expression was upregulated in *Pkd1* mutant cystic epithelial cells (4); and that MIF induced the expression of MCP-1 and TNF-α in *Pkd1* mutant renal epithelial cells (Supplemental Figure 12) suggest that *Pkd1* mutant renal epithelial cells might be another source for the origin of chemoattractants, which are regulated by MIF in ADPKD kidneys. MIF induces macrophage recruitment through chemokine CCL2 (MCP-1) and through monocyte recruitment cytokines, including TNF-α, IL-1β, and IL-2, which were found in cyst fluids from human kidneys (26). KO of MIF or inhibition of MIF with ISO-1 diminished the levels of macrophages present within pericystic and interstitial regions of *Pkd1* KO mouse kidneys (Supplemental Figure 5) and reduced migration of human THP-1 monocytes in vitro (Supplemental Figure 9). These results suggest that MIF contributes to the recruitment of macrophages in the cystic kidneys of *Pkd1* KO mice (Figure 8). Whether MIF recruits renal macrophages directly in vivo or through its effects on MCP-1 and/or TNF-α signaling is unknown.

The metabolic effects of MIF. MIF induces cellular glucose uptake and stimulates glycolysis during sepsis (40). It has been suggested that *Pkd1*-deficient cells reprogram their glucose metabolism to use aerobic glycolysis (33), a phenomenon often called the Warburg effect, which has been recognized in cancer for more than 80 years (47). Warburg's observation indicates that unlike most of the normal cells, which channel pyruvate into the tricarboxylic acid (TCA) cycle, cancer cells preferentially generate energy through "fermenting" glucose into lactate and reducing pyruvate into lactate, even in the presence of sufficient oxygen. Due to the lower efficiency of aerobic glycolysis in terms of ATP production per glucose molecule versus the TCA cycle, a definitive explanation for Warburg's observation has remained elusive, at least in part because the energy requirements of cell proliferation appear at first glance to be better met by complete catabolism of glucose using mitochondrial oxidative phosphorylation to maximize ATP production. It has been proposed that the metabolism of cancer cells, and indeed all proliferating cells, is adapted to facilitate the uptake and incorporation of nutrients, particularly glucose, that meet or exceed the bioenergetic demands of cell growth and proliferation (48). The reported finding that the cystic kidneys from *Pkd1*^{fl/-} *Ksp-Cre* mice showed a higher uptake of glucose and more conversion to lactate compared with control kidneys (33), and our results that glucose uptake was increased in Pkd1 mutant renal epithelial cells (Figure 5A) not only suggested a switch to the Warburg effect but also supported this prediction. PKD1 mutation–mediated glycolysis may depend on ERK-mediated inhibition of AMPK and activation of the mTOR-glycolytic cascade (33). However, the upstream factor(s) that regulate the uptake of glucose have not been explored in ADPKD. Based on our observation that MIF not only regulated the uptake of glucose and the generation of ATP in renal epithelial cells (Figure 5), but also activated ERK and mTOR signaling and inhibited the AMPK pathway in *Pkd1* mutant renal epithelial cells and tissues (Figure 6), we think that MIF is a key upstream activator of all of these processes and pathways and may act in a dual mechanism to inhibit AMPK in *Pkd1* mutant renal epithelial cells. MIF may induce glucose uptake to directly increase glycolysis and the generation of ATP, which then acts to inhibit the activation of AMPK. MIF-mediated activation of ERK signaling is likely to activate the mTOR-glycolytic cascade, as has been proposed (33), which also inhibits the activation of AMPK. Inhibition of AMPK will relieve its inhibition on ERK or mTOR (23) to form double feedback loops to increase cystic epithelial cell proliferation (Figure 8). Activation of ERK signaling promotes cyst growth (35), while targeting mTOR with rapamycin or activating AMPK with metformin delays cyst growth in several different models of ADPKD (30, 31). Although the interaction among the mechanisms involved remains elusive, our results favor the view that MIF impacts defective glucose metabolism, ATP generation and cyst epithelial cell proliferation by mediating the interplay among ERK, mTOR, and AMPK in ADPKD.

MIF and its receptor CD74-mediated pathways. MIF promotes either the transient or the sustained activation of ERK1/2 mitogen–activated protein kinase (MAPK) pathway (20, 21), and this process is dependent on MIF interaction with its membrane receptor, CD74 (49). We found that the expression of CD74 was upregulated in *Pkd1* mutant renal epithelial cells (Supplemental Figure 16,

A and B) and was elevated in ADPKD kidneys (Supplemental Figure 16C). We also found that MIF induced rapid and transient activation of ERK in *Pkd1* mutant renal epithelial cells in vitro (Figure 6, A and B) but sustained activation of ERK in *Pkd1* KO mouse kidneys in vivo (Figure 6, E and F). We further found that treatment with CD74 antibody blocked the MIF-induced the phosphorylation of ERK but did not affect the MIF-induced MCP-1 expression (Supplemental Figure 16D). It has been reported that activation of the ERK/MAPK signaling pathway by MIF in fibroblasts and macrophages is dependent on SRC kinase activity (21), which suggests that MIF is an upstream regulator of SRC-mediated ERK MAPK signaling. Inhibition of SRC kinase activity delayed renal cyst growth in PKD animal models (50). Whether activation of ERK by MIF is dependent on CD74-mediated activation of SRC or other mechanisms in cystic renal epithelial cells awaits investigation. In addition, CD74 is responsible for signaling to AMPK activation by MIF (22), since silencing CD74 with siRNA had the same effects of enhanced AMPK phosphorylation as MIF silencing with siRNA in non–small cell lung carcinomas cells (23). The elevation of CD74 in *Pkd1* mutant renal epithelial cells and ADPKD kidneys (Supplemental Figure 16) implies that MIF may also signal through CD74 to inhibit AMPK phosphorylation and activity in those cells.

MIF and the p53 pathway. MIF has been described as an inhibitor of p53-dependent apoptosis in macrophages (51). It was hypothesized that upregulation of MIF at sites of chronic inflammation might impair p53-dependent cellular responses toward DNA damage and induce inappropriate proliferation and, thus, promote the accumulation of oncogenic mutations (52). We found that inhibition of MIF with ISO-1–induced p53-dependent *Pkd1* mutant renal epithelial cell apoptosis, since knockdown of p53 abolished ISO-1–induced cell death in these cells (Figure 7); this suggested that, in addition to its effects on macrophages, MIF also regulated p53-dependent cystic renal epithelial cell death. However, the mechanisms for the upregulation of p53 and the activation of caspase-3 in *Pkd1* mutant renal epithelial cells upon ISO-1 treatment remain to be determined.

Methods

Cell culture and reagents. *Pkd1* WT and *Pkd1* null MEK cells, which were generated from Jing Zhou's laboratory at Harvard Medical School (Boston, Massachusetts, USA) and were used in our recent publications, were maintained as previously described (2, 53). *Pkd1* heterozygous PH2 cells and homozygous PN24 cells, provided by Stefan Somlo through the George M. O'Brien Kidney Center at Yale University (New Haven, Connecticut, USA), were cultured as described (35, 54). ISO-1 was purchased from EMD Millipore. Recombinant mouse MIF was purchased from R&D Systems. *Pkd1* null MEK cells and PN24 cells were treated with ISO-1 or recombinant MIF for 24 hours and then were harvested and analyzed by Western blot. The CM from *Pkd1* null MEK cells transfected with control siRNA or MIF siRNA for 72 hours were collected by centrifuging at 3,000 *g* for 10 minutes and then used to stimulate the *Pkd1* null MEK cells and PN24 cells. PN24 cells were pretreated with normal IgG or CD74 antibody for 2 hours and then treated with recombinant MIF (10 ng/ml), and the whole cell lysates were analyzed by Western blot. *Pkd1* WT MEK cells treated with or without ISO-1, as well as the cells transfected with p53 siRNA or MIF siRNA for 24 hours, were analyzed by TUNEL

assay. The *Pkd1* null MEK cells with p53 siRNA or control siRNA transfection for 24 hours were treated with ISO-1 or transfected with MIF siRNA for another 24 hours and analyzed by TUNEL assay. Primary cells obtained from the cavities of cysts on the surfaces of ADPKD kidneys (ADPKD cells) were supplied by the PKD Research Biomaterials and Cellular Models Core at the KUMC (Kansas City, Kansas, USA) and cultured up to 3 passages in DMEM/F-12 (Cellgro 15-090-CV; Corning) supplemented with 5% FBS, 15 mM HEPES, 5 μg/ml insulin, 5 μg/ml transferrin, and 5 ng/ml sodium selenite (ITS; BD Biosciences) plus penicillin (100 U/ml), streptomycin (Pen/Strep; 130 μg/ml). CM was prepared from ADPKD cells incubated in DMEM (Sigma-Aldrich) containing 10% FBS, 2 mM additional glutamine, and Pen/Strep for 3 days. THP-1 monocytes were maintained in RPMI-1640 media (Sigma-Aldrich) containing 10% FBS, 2mM L-glutamine, and Pen/Strep.

Subcellular fractionation. The *Pkd1* null MEK cells were washed twice with PBS and harvested by scraping, followed by centrifugation. The cell pellets were resuspended in 10 volumes of Buffer A, containing 2.0 mM $MgCl_2$, 25 mM KCl, 10 mM HEPES (pH 7.5), and protease inhibitors. Cells were homogenized in a homogenizer after swelling for 10 minutes on ice. The homogenate was centrifuged at 1,000 *g* for 10 minutes to generate the first pellets and the first supernatant. The first pellets — which were resuspended in 3 ml of Buffer N, containing 0.25 M sucrose in buffer A, and were layered over 2 ml of medium containing 1.1 M sucrose in buffer A — were centrifuged at 1,000 *g* for 10 minutes to collect the nuclear pellet. The first supernatant was further fractionated by centrifugation at 35,000 *g* for 40 minutes to generate the second pellets and the second supernatant. The second supernatant represented soluble cytoplasmic proteins, whereas the second pellets contained plasma membrane proteins. The nuclei, cytoplasmic, and plasma membrane fractions were resuspended in SDS sample buffer for Western blot analysis.

Western blot analysis. We performed Western blotting on whole-cell lysates as previously described (53). Briefly, cells were lysed at 4°C with RIPA buffer consisting of 20 mM Tris-HCl (pH 7.5), 1% Triton X-100, 150 mM NaCl, 1% glycerol, 0.5 mM dithiothreitol, and 1 mM sodium vanadate plus protease inhibitor (Roche Applied Science). The protein in the cell lysates were analyzed by blotting with the following primary antibodies: anti–phospho-Rb (#9307), anti-p53 (#2524), anti-AKT (#9272), anti–phospho-Akt (#9271), anti-S6 (#2217), anti–phospho-S6 (#2211), anti-AMPK (#9831), anti–phospho-AMPK (#2531), anti-ERK (#9107), anti–phospho-ERK (#9101), anti-PARP (#9542), anti–active caspase-3 antibodies (#9661), anti–Lamin A/C (#2032), anti–Na/K ATPase (#3010; Cell Signaling Technologies; 1:1,000 dilution); anti-actin antibody (A2228; Sigma-Aldrich; 1:5,000 dilution); and anti-Rb (SC-7905), anti-MCP-1(SC-1785), anti–TNF-α (SC-52746), anti-MIF (SC-20121), and anti-CD74 (SC-20082) antibodies (Santa Cruz Biotechnology; 1:200–500 dilution). Donkey anti-rabbit IgG–horseradish peroxidase, donkey anti-mouse IgG–horseradish peroxidase, and donkey anti-goat IgG–horseradish peroxidase (Santa Cruz Biotechnology; 1:8,000 dilution) were used as secondary antibodies.

Immunohistochemistry. Kidneys were fixed with 4% paraformaldehyde (pH7.4). For PCNA, MIF, and MCP-1 staining, the primary antibodies, including mouse anti-PCNA antibody (2586; Cell Signaling Technology; 1:1,000 dilution), rabbit anti-MIF antibody (SC-20121; Santa Cruz Biotechnology; 1:100 dilution), and goat anti–MCP-1 antibody (SC-1785; Santa Cruz Biotechnology; 1:100 dilution); the perox-

idase labeled secondary anti-mouse, -rabbit, and -goat IgG secondary antibodies (Sigma-Aldrich); and DAB substrate system were used. Kidney sections were counterstained by haematoxylin. The exposure time of the slides to the reagents was the same for the samples of all groups in each independent experiment. Images were analyzed with a NIKON ECLIPSE 80i microscope.

Immunofluorescence staining. Macrophages were detected by immunofluorescence staining (IF staining) with a pan-macrophage marker, F4/80. After antigen retrieval, tissue sections were incubated with a rat anti-mouse F4/80 antibody (14-4801-82; eBioscience Inc.; 1:100 dilution) overnight, and then were incubated with Fluro-555 anti-rat IgG secondary antibody and mounted in Prolong Gold Anti-fade reagent with DAPI (Invitrogen). For Ki67 staining, a rabbit anti-Ki67 antibody (ab15580; Abcam) and Fluro-488 anti-rabbit IgG secondary antibody were used. Images were analyzed using a NIKON ECLIPSE 80i microscope.

Quantitative reverse-transcription PCR (qRT-PCR). The RNA extraction and reverse transcription were performed as previous described (2). RNA expression profiles were analyzed by real-time PCR using iTaq SYBER Green Supermix (Bio-Rad) in a CFX Connect real-time PCR detection system (Bio-Rad). Genes were amplified using the following primers: *Mif*-F, 5′-AGAACCGCAACTACAGTAAGC-3′; *Mif*-R, 5′-ACTCAAGCGAAGGTGGAAC-3′; *Hk1*-F, 5′-TCACATTGTCTCCT-GCATCTC-3′; *Hk1*-R, 5′-CTTTGAATCCCTTTGTCCACG-3′; *Ldha*-F, 5′-GCTCCCCAGAACAAGATTACAG-3′; *Ldha*-R, 5′-TCGCCCTT-GAGTTTGTCTTC-3′; *Pkm2*-F, 5′-CCATTCTCTACCGTCCTGTTG-3′; *Pkm2*-R, 5′-TCCATGTAAGCGTTGTCCAG-3′; *actin*-F, 5′-AAGAGC-TATGAGCTGCCTGA-3′; *actin*-R, 5′-TACGGATGTCAACGTCA-CAC-3′. The complete reactions were subjected to the following program of thermal cycling: 40 cycles of 10 seconds at 95°C and 20 seconds at 61°C. A melting curve was run after the PCR cycles, followed by a cooling step. Each sample was run in triplicate in each experiment, and each experiment was repeated 3 times. Expression levels of *Mif*, *Hk1*, *Ldha*, and *Pkm2* were normalized to the expression level of actin.

Migration assay. Cell migration assays were carried out using 8 μm pore size transwells in 24-well plates. Lower wells contained 600 μl media alone (DMEM containing 10% FBS, 2 mM additional glutamine, and Pen/Strep) or ADPKD cyst cell CM, and upper insert wells were seeded with THP-1 monocytes (100 μl of 1×10^6 cells) prior to incubation for 18 hours at 37°C. Inserts were then discarded, and migrated cells were collected from the lower wells, pelleted by centrifugation at 600 *g* for 5 minutes, and frozen at –80°C prior to lysis in buffer containing CyQUANT GR dye (Invitrogen), according to the manufacturer's directions. Quantitative measurement of fluorescence was carried out using a SynergyTM 2 microplate reader (BioTek Instruments Inc.). Values for the total number of cells seeded were obtained by quantifying in parallel pelleted, frozen 100 μl aliquots of the original cell suspension.

RNA interference. The RNA oligonucleotides that specifically targeted mouse MIF and mouse p53 were purchased from GE Healthcare and Santa Cruz Biotechnology Inc., respectively. The RNA oligonucleotides were transfected with DharmaFECT siRNA transfection reagent (GE Healthcare). 24 hours after transfection, cells were harvested and analyzed by Western blotting.

Glucose uptake assay. The medium of cells transfected with MIF siRNA for 24 hours was replaced with fresh medium. After an additional 24 hours of incubation, the remaining glucose in the cell medium

was analyzed using the Amplex Red glucose assay kit (Invitrogen), according to the manufacturer's protocol. Glucose uptake was shown by subtracting the remaining glucose from total glucose in the fresh medium. For ISO-1 treatment, the cells treated by ISO-1 for 24 hours were replaced with fresh medium with ISO-1. After an additional 24 hours of incubation, the glucose was analyzed as described above.

ATP assay. The cells were transfected with MIF siRNA or ISO-1 for 48 hours and lysed by RIPA buffer. The intracellular ATP levels of cell lysates were assessed using the ATP Determination Kit (Invitrogen), according to the manufacturer's protocol. The intracellular ATP levels were shown by normalizing to protein amount.

TUNEL assay. TUNEL assay for *Pkd1* WT MEK cells, *Pkd1* null MEK cells, and kidneys treated with ISO-1 or DMSO were performed according to the manufacturer's protocols (In Situ Death Detection Kit; Roche Diagnostics). ProLong Gold Antifade reagent with DAPI (Invitrogen) was used. IF images were obtained with a NIKON ECLIPSE 80i microscope.

Mouse strain and treatment. *Pkd1*$^{fl/fl}$ *Ksp-Cre* mice were used to test the effect of ISO-1 on cyst progression at PN7. *Pkd1*$^{fl/fl}$ mice and *Ksp-Cre* transgenic mice were generated as described previously (35, 55). *Pkd1*$^{fl/fl}$ (C57BL/6; 129S4-*Pkd1*^{tm2Ggg}/J [Stock 010671]; The Jackson Laboratory) mice possess loxP site on either side of exon 2–4 of the *Pkd1* gene (35). *Ksp-Cre* mice express Cre recombinase under the control of the *Ksp*-cadherin promoter (55). *Pkd1*$^{fl/fl}$ *Ksp-Cre* mice were generated by cross-breeding *Pkd1*$^{fl/+}$ *Ksp-Cre* female mice with *Pkd1*$^{fl/+}$ *Ksp-Cre* male mice. Each neonate was i.p. injected daily with 35 mg/kg ISO-1 or DMSO from PN3–PN6. Littermate controls were used in all animal experiments.

Pkd1$^{fl/fl}$ *Pkhd1-Cre* mice were used to test the effect of ISO-1 on cyst progression at P25 (6). *Pkd1*$^{fl/fl}$ *Pkhd1-Cre* mice were generated by cross-breeding *Pkd1*$^{fl/+}$ *Pkhd1-Cre* female mice with *Pkd1*$^{fl/+}$ *Pkhd1-Cre* male mice. Each neonate was i.p. injected daily with 35 mg/kg ISO-1 or DMSO from PN9–PN24. The kidneys were harvested and analyzed at PN25. Littermate controls were used in all animal experiments.

Hypomorphic *Pkd1*$^{nl/nl}$ mice, generated by cross-breeding *Pkd1*$^{nl/+}$ females with *Pkd1*$^{nl/+}$ males, were used to test the effect of ISO-1 on cyst growth at PN28. Each neonate was i.p. injected daily with 35 mg/kg ISO-1 or DMSO from PN5–PN27, and the kidneys were harvested at P28 for further analysis.

Mif KO mice (Mif$^{-/-}$*)* were used to generate *Mif* and *Pkd1* double KO *Pkd1*$^{fl/fl}$ *Ksp-Cre Mif*$^{-/-}$ mice. The *Mif*$^{-/-}$ mice were not conditional KO mice; they developed normally in size and behavior, and they were fertile (56). *Pkd1*$^{fl/+}$ *Ksp-Cre Mif*$^{+/-}$ mice were generated by crossing

Pkd1$^{fl/fl}$ *Ksp-Cre* male mice with *Mif*$^{-/-}$ female mice. *Pkd1*$^{fl/fl}$ *Ksp-Cre Mif*$^{-/-}$ mice were generated by crossing *Pkd1*$^{fl/+}$ *Ksp-Cre Mif*$^{-/-}$ male mice with *Pkd1*$^{fl/+}$ *Ksp-Cre Mif*$^{+/-}$ female mice. *Pkd1*$^{fl/fl}$ mice, *Pkd1*$^{fl/fl}$ *Ksp-Cre* mice, and *Mif*$^{-/-}$ mice were on the C57BL/6 genetic background. In *Pkd1*$^{fl/fl}$ *Ksp-Cre Mif*$^{-/-}$ mice, *Pkd1* should be conditionally knocked out in tubular epithelial cells of kidneys, whereas *Mif* should be knocked out in all kinds of renal cells and other organs.

Statistics. Data are presented as mean ± SEM. Unpaired 2-tailed Student's *t* test was used to determine significance of differences between 2 groups. One-way ANOVA post hoc test (IBM SPSS Version 22.0) was used to determine significance of differences in the variables among multiple groups. *P* values less than 0.05 were considered significant.

Study approval. All animal protocols were approved and conducted in accordance with Laboratory Animal Resources of KUMC (Kansas City, Kansas, USA) and Institutional Animal Care and Use Committee regulations (Protocol #2012-2092).

Urine specimens were obtained from the KUMC PKD Repository, which is a biobank approved by the institutional review board at the KUMC, Kansas City, Kansas, USA, in accordance with FDA code 21 CFR 56. ADPKD patients and normal volunteers provided informed consent prior to the collection of urine and medical information. Urine samples and data were de-identified. ADPKD tissue and primary cells obtained from the PKD Research Biomaterial and Cellular Models Core are not considered human subjects, since the specimens were removed for clinical reasons and were de-identified.

Acknowledgments

Address correspondence to: Xiaogang Li, Department of Internal Medicine, and the Kidney Institute, KUMC, Mail Stop 3018, 3901 Rainbow Blvd., Kansas City, Kansas 66160, USA. Phone: 913.588.2731; E-mail: xli3@kumc.edu.

1. Harris PC. Autosomal dominant polycystic kidney disease: clues to pathogenesis. *Hum Mol Genet*. 1999;8(10):1861–1866.
2. Zhou X, et al. Sirtuin 1 inhibition delays cyst formation in autosomal-dominant polycystic kidney disease. *J Clin Invest*. 2013;123(7):3084–3098.
3. Fan LX, Li X, Magenheimer B, Calvet JP, Li X. Inhibition of histone deacetylases targets the transcription regulator Id2 to attenuate cystic epithelial cell proliferation. *Kidney Int*. 2012;81(1):76–85.
4. Fan LX, et al. Smac-mimetic–induced epithelial cell death reduces the growth of renal cysts. *J Am Soc Nephrol*. 2013;24(12):2010–2022.
5. Swenson-Fields KI, et al. Macrophages promote polycystic kidney disease progression. *Kidney Int*. 2013;83(5):855–864.
6. Karihaloo A, et al. Macrophages promote cyst growth in polycystic kidney disease. *J Am Soc Nephrol*. 2011;22(10):1809–1814.
7. Lolis E, Bucala R. Macrophage migration inhibitory factor. *Expert Opin Ther Targets*. 2003;7(2):153–164.
8. Calandra T, Roger T. Macrophage migration inhibitory factor: a regulator of innate immunity. *Nat Rev Immunol*. 2003;3(10):791–800.
9. Bacher M, et al. An essential regulatory role for macrophage migration inhibitory factor in T-cell activation. *Proc Natl Acad Sci U S A*. 1996;93(15):7849–7854.
10. Calandra T, Bernhagen J, Mitchell RA, Bucala R. The macrophage is an important and previously unrecognized source of macrophage migration inhibitory factor. *J Exp Med*. 1994;179(6):1895–1902.
11. Nishihira J, Koyama Y, Mizue Y. Identification of macrophage migration inhibitory factor (MIF) in human vascular endothelial cells and its induction by lipopolysaccharide. *Cytokine*. 1998;10(3):199–205.
12. Imamura K, et al. Identification and immunohistochemical localization of macrophage migration

inhibitory factor in human kidney. *Biochem Mol Biol Int*. 1996;40(6):1233–1242.

13. Chen Z, et al. Evidence for a role of macrophage migration inhibitory factor in vascular disease. *Arterioscler Thromb Vasc Biol*. 2004;24(4):709–714.

14. Kasama T, Ohtsuka K, Sato M, Takahashi R, Wakabayashi K, Kobayashi K. Macrophage migration inhibitory factor: a multifunctional cytokine in rheumatic diseases. *Arthritis*. 2010;2010:106202.

15. Morimoto T, Nishihira J, Kohgo T. Immunohistochemical localization of macrophage migration inhibitory factor (MIF) in human gingival tissue and its pathophysiological functions. *Histochem Cell Biol*. 2003;120(4):293–298.

16. Lan HY. Role of macrophage migration inhibition factor in kidney disease. *Nephron Exp Nephrol*. 2008;109(3):e79–e83.

17. Matsumoto K, Kanmatsuse K. Increased production of macrophage migration inhibitory factor by T cells in patients with IgA nephropathy. *Am J Nephrol*. 2001;21(6):455–464.

18. Lan HY, et al. TNF-alpha up-regulates renal MIF expression in rat crescentic glomerulonephritis. *Mol Med*. 1997;3(2):136–144.

19. Hoi AY, et al. Macrophage migration inhibitory factor deficiency attenuates macrophage recruitment, glomerulonephritis, and lethality in MRL/lpr mice. *J Immunol*. 2006;177(8):5687–5696.

20. Mitchell RA, Metz CN, Peng T, Bucala R. Sustained mitogen-activated protein kinase (MAPK) and cytoplasmic phospholipase A2 activation by macrophage migration inhibitory factor (MIF). Regulatory role in cell proliferation and glucocorticoid action. *J Biol Chem*. 1999;274(25):18100–18106.

21. Lue H, et al. Rapid and transient activation of the ERK MAPK signalling pathway by macrophage migration inhibitory factor (MIF) and dependence on JAB1/CSN5 and Src kinase activity. *Cell Signal*. 2006;18(5):688–703.

22. Miller EJ, et al. Macrophage migration inhibitory factor stimulates AMP-activated protein kinase in the ischaemic heart. *Nature*. 2008;451(7178):578–582.

23. Brock SE, Rendon BE, Yaddanapudi K, Mitchell RA. Negative regulation of AMP-activated protein kinase (AMPK) activity by macrophage migration inhibitory factor (MIF) family members in non-small cell lung carcinomas. *J Biol Chem*. 2012;287(45):37917–37925.

24. Fingerle-Rowson G, et al. The p53-dependent effects of macrophage migration inhibitory factor revealed by gene targeting. *Proc Natl Acad Sci U S A*. 2003;100(16):9354–9359.

25. Toh ML, et al. Regulation of IL-1 and TNF receptor expression and function by endogenous macrophage migration inhibitory factor. *J Immunol*. 2006;177(7):4818–4825.

26. Gregory JL, et al. Macrophage migration inhibitory factor induces macrophage recruitment via CC chemokine ligand 2. *J Immunol*. 2006;177(11):8072–8079.

27. Lue H, et al. Macrophage migration inhibitory factor (MIF) promotes cell survival by activation of the Akt pathway and role for CSN5/JAB1 in the control of autocrine MIF activity. *Oncogene*. 2007;26(35):5046–5059.

28. Petrenko O, Moll UM. Macrophage migration inhibitory factor MIF interferes with the Rb-E2F pathway. *Mol Cell*. 2005;17(2):225–236.

29. Takiar V, et al. Activating AMP-activated protein kinase (AMPK) slows renal cystogenesis. *Proc Natl Acad Sci U S A*. 2011;108(6):2462–2467.

30. Shillingford JM, et al. The mTOR pathway is regulated by polycystin-1, and its inhibition reverses renal cystogenesis in polycystic kidney disease. *Proc Natl Acad Sci U S A*. 2006;103(14):5466–5471.

31. Shillingford JM, Leamon CP, Vlahov IR, Weimbs T. Folate-conjugated rapamycin slows progression of polycystic kidney disease. *J Am Soc Nephrol*. 2012;23(10):1674–1681.

32. Li X, et al. A tumor necrosis factor-alpha-mediated pathway promoting autosomal dominant polycystic kidney disease. *Nat Med*. 2008;14(8):863–868.

33. Rowe I, et al. Defective glucose metabolism in polycystic kidney disease identifies a new therapeutic strategy. *Nat Med*. 2013;19(4):488–493.

34. Zheng D, et al. Urinary excretion of monocyte chemoattractant protein-1 in autosomal dominant polycystic kidney disease. *J Am Soc Nephrol*. 2003;14(10):2588–2595.

35. Shibazaki S, et al. Cyst formation and activation of the extracellular regulated kinase pathway after kidney specific inactivation of Pkd1. *Hum Mol Genet*. 2008;17(11):1505–1516.

36. Al-Abed Y, VanPatten S. MIF as a disease target: ISO-1 as a proof-of-concept therapeutic. *Future Med Chem*. 2011;3(1):45–63.

37. Leuenroth SJ, Bencivenga N, Igarashi P, Somlo S, Crews CM. Triptolide reduces cystogenesis in a model of ADPKD. *J Am Soc Nephrol*. 2008;19(9):1659–1662.

38. Lantinga-van Leeuwen IS, et al. Lowering of Pkd1 expression is sufficient to cause polycystic kidney disease. *Hum Mol Genet*. 2004;13(24):3069–3077.

39. Cowley BD, Cowley BD Jr, Ricardo SD, Nagao S, Diamond JR. Increased renal expression of monocyte chemoattractant protein-1 and osteopontin in ADPKD in rats. *Kidney Int*. 2001;60(6):2087–2096.

40. Benigni F, et al. The proinflammatory mediator macrophage migration inhibitory factor induces glucose catabolism in muscle. *J Clin Invest*. 2000;106(10):1291–1300.

41. Sanchez-Nino MD, et al. MIF, CD74 and other partners in kidney disease: tales of a promiscuous couple. *Cytokine Growth Factor Rev*.

2013;24(1):23–40.

42. Bernhagen J, et al. MIF is a noncognate ligand of CXC chemokine receptors in inflammatory and atherogenic cell recruitment. *Nat Med*. 2007;13(5):587–596.

43. Grantham JJ, Mulamalla S, Swenson-Fields KI. Why kidneys fail in autosomal dominant polycystic kidney disease. *Nat Rev Nephrol*. 2011;7(10):556–566.

44. Seeger-Nukpezah T, et al. Inhibiting the HSP90 chaperone slows cyst growth in a mouse model of autosomal dominant polycystic kidney disease. *Proc Natl Acad Sci U S A*. 2013;110(31):12786–12791.

45. Schulz R, et al. Inhibiting the HSP90 chaperone destabilizes macrophage migration inhibitory factor and thereby inhibits breast tumor progression. *J Exp Med*. 2012;209(2):275–289.

46. Rees AJ. Monocyte and macrophage biology: an overview. *Semin Nephrol*. 2010;30(3):216–233.

47. Warburg O. On the origin of cancer cells. *Science*. 1956;123(3191):309–314.

48. Vander Heiden MG, Cantley LC, Thompson CB. Understanding the Warburg effect: the metabolic requirements of cell proliferation. *Science*. 2009;324(5930):1029–1033.

49. Leng L, et al. MIF signal transduction initiated by binding to CD74. *J Exp Med*. 2003;197(11):1467–1476.

50. Sweeney WE, Sweeney WE Jr, von Vigier RO, Frost P, Avner ED. Src inhibition ameliorates polycystic kidney disease. *J Am Soc Nephrol*. 2008;19(7):1331–1341.

51. Mitchell RA, et al. Macrophage migration inhibitory factor (MIF) sustains macrophage proinflammatory function by inhibiting p53: regulatory role in the innate immune response. *Proc Natl Acad Sci U S A*. 2002;99(1):345–350.

52. Hudson JD, Shoaibi MA, Maestro R, Carnero A, Hannon GJ, Beach DH. A proinflammatory cytokine inhibits p53 tumor suppressor activity. *J Exp Med*. 1999;190(10):1375–1382.

53. Li X, Luo Y, Starremans PG, McNamara CA, Pei Y, Zhou J. Polycystin-1 and polycystin-2 regulate the cell cycle through the helix-loop-helix inhibitor Id2. *Nat Cell Biol*. 2005;7(12):1202–1212.

54. Wei F, et al. Neutrophil gelatinase-associated lipocalin suppresses cyst growth by Pkd1 null cells in vitro and in vivo. *Kidney Int*. 2008;74(10):1310–1318.

55. Shao X, Somlo S, Igarashi P. Epithelial-specific Cre/lox recombination in the developing kidney and genitourinary tract. *J Am Soc Nephrol*. 2002;13(7):1837–1846.

56. Gadjeva M, Nagashima J, Zaidi T, Mitchell RA, Pier GB. Inhibition of macrophage migration inhibitory factor ameliorates ocular Pseudomonas aeruginosa-induced keratitis. *PLoS Pathog*. 2010;6(3):e1000826.